

Fiber-Tip Polymer Microcantilever for Fast and Highly Sensitive Hydrogen Measurement

Cong Xiong, Jiangtao Zhou, Changrui Liao,* Meng Zhu, Ying Wang, Shen Liu, Chi Li, Yunfang Zhang, Yuanyuan Zhao, Zongsong Gan, Leonardo Venturelli, Sandor Kasas, Xuming Zhang, Giovanni Dietler,* and Yiping Wang



Cite This: *ACS Appl. Mater. Interfaces* 2020, 12, 33163–33172



Read Online

ACCESS |

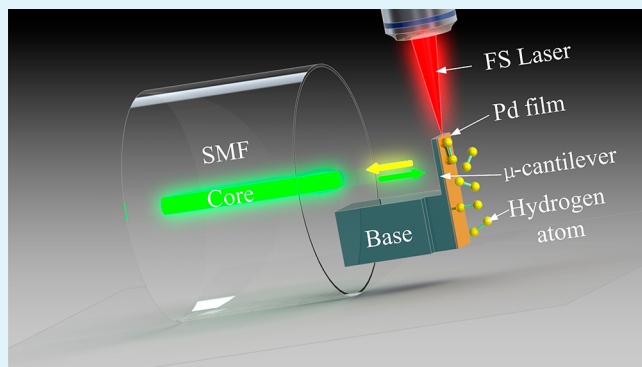
Metrics & More

Article Recommendations

Supporting Information

ABSTRACT: Hydrogen as an antioxidant gas has been widely used in the medical and biological fields for preventing cancer or treating inflammation. However, controlling the hydrogen concentration is crucial for practical use due to its explosive property when its volume concentration in air reaches the explosive limit (4%). In this work, a polymer-based microcantilever (μ -cantilever) hydrogen sensor located at the end of a fiber tip is proposed to detect the hydrogen concentration in medical and biological applications. The proposed sensor was developed using femtosecond laser-induced two-photon polymerization (TPP) to print the polymer μ -cantilever and magnetron sputtering to coat a palladium (Pd) film on the upper surface of the μ -cantilever. Such a device exhibits a high sensitivity, roughly $-2 \text{ nm } \text{%}^{-1}$ when the hydrogen concentration rises from 0% to 4.5% (v/v) and a short response time, around 13.5 s at 4% (v/v), making it suitable for medical and environmental applications. In addition to providing an ultracompact optical solution for fast and highly sensitive hydrogen measurement, the polymer μ -cantilever fiber sensor can be used for diverse medical and biological sensing applications by replacing Pd with other functional materials.

KEYWORDS: optical fiber sensor, hydrogen measurement, microcantilever, palladium film, femtosecond laser micromachining, two-photon polymerization



1. INTRODUCTION

Hydrogen is a high-quality antioxidant that is used in the frame of several diseases and can be given by simply breathing, drinking, or through the injection of hydrogen-containing liquids. Hydrogen has been effectively used in the treatment of animal skin malignancies, and the direct reaction of hydrogen with hydroxyl radicals is the basis of treating inflammatory injuries.¹ Extensive *in vivo* studies documented that hydrogen also shows beneficial effects in regard to the treatment of various diseases, such as brain or lung injuries and Parkinson's disease.^{2,3} Therefore, hydrogen will probably play an important role in future medical and biological research. In addition to biomedical applications, hydrogen is a promising candidate for a next-generation clean energy carrier. However, large safety concerns are associated with the transportation, storage, and usage of hydrogen due to its extremely explosive properties in air when its volume concentration reaches the explosive limit of 4%. Thus, the development of a sensitive and rapid hydrogen detection method is of great significance in many energy, medical, and biological applications. Commercial hydrogen sensors based on resistance, both electrochemical and microelectromechanical, are still demodulated with an

electrical signal so that there is the potential risk of an explosion triggered by an electric spark during the electrical signal readout.^{4–6} Optical fibers as a low-cost ultracompact platform have been widely used in biochemical research.^{7–12} Compared with the electrical ones, the optical sensors are much more suitable for an explosive environment due to the absence of electrical arcing, avoiding the risk of detonation and electromagnetic interference.^{13–15} Over the past few decades, various types of hydrogen sensors have been investigated, such as surface plasma resonance (SPR) architectures,^{16–18} fiber evanescent field structures,^{19–21} optical fiber interferometers,^{22,23} and fiber Bragg gratings (FBGs).^{24,25} SPR architectures need expensive instruments to precisely control the thickness of the metal film, which complicates the manufac-

Received: April 3, 2020

Accepted: June 4, 2020

Published: June 4, 2020



ing process. Fiber evanescent field structures usually require tapering or side polishing of the optical fiber to enhance the evanescent field; this process decreases the robustness of the sensor. The sensitivity of FBG hydrogen sensors is usually only at the pm %⁻¹ level. The decoration of Pd nanoparticles on the whispering gallery mode (WGM) device or a nanoantenna has enabled sensitive H₂ detection by measuring the change in the localized surface plasmon resonance (LSPR) of the nanoparticle.^{26,27} However, it is necessary to cope with the weak LSPR signals, and the excitation and detection schemes are complicated. For a femtosecond laser-carved Fabry-Pérot (FP) cavity coated with Pd film, the film expansion induced by absorbing H₂ gives rise to a cavity length change.²⁸ Although this method deals with a strong signal and a compact scheme, a micrometer-thickness Pd film is needed to improve the sensitivity due to the stiffness limitation of silica fiber, and the thick film will significantly slow the sensor response.

In order to make hydrogen sensors fitting for medical and biological practical uses, it is necessary to downsize them to a portable size so that they can be inserted into the gas microchannel. TPP 3D lithography by a near-infrared femtosecond (fs) laser has been widely used in photonics,^{29–34} micromachines,^{35,36} microfluidics,^{37–39} and biomedicine.^{40,41} Even functional materials that are difficult to manufacture, such as miniature biomimetic or nanogap plasmonic structures, have been significantly developed thanks to the high machining accuracy and flexibility of TPP technology.^{42,43} This nanomachining technology increases the possibilities of using the facet of the optical fiber as an inherently light-coupled microscopic platform to create new functions for fiber-based devices. By combining TPP technology and the concept of “lab on fiber”, it becomes possible to develop novel μ -probe sensors. For example, this technology enabled the fabrication of a 3D surface-enhanced Raman scattering (SERS) sensor on the facet of an optical fiber,²⁹ a miniature wide-spectrum mode sorter for vortex beams,³⁰ an integrated (de)multiplexer,⁴⁴ and multilens objectives.⁴⁵

The precise readout of the conventional cantilever deflection is typically undertaken using an optical lever technique similar to that used in an atomic force microscopy (AFM) readout.⁴⁶ First, the sensing part is separated from the light source and the collection device. It makes the sensor system bulky and cumbersome, which is not conducive to measurements in space-limited environments. Furthermore, optical signal loss is serious due to the use of spatial light transmission and collection, which makes the environmental noise have a great impact on the sensor accuracy. In order to make cantilever-based sensors fitting for medical and biological practical uses, it is necessary to downsize them to a portable size and reduce the impact of environmental noise on the sensors.

In this paper, we integrate the fiber and the cantilever together by TPP to form a highly integrated cantilever-based fiber sensor. It not only realizes the simplicity of the sensor but also reduces the optical signal loss in the transmission by the use of a fiber-tip FP interferometer (FPI) that takes the fiber as the medium of light transmission and collection. The hydrogen fiber sensor based on a polymer microcantilever (μ -cantilever) printed by TPP on the end face of single mode fiber (SMF) is presented (Figure 1). Both the suspended μ -cantilever parallel to the fiber end face and the base for supporting it are printed on the SMF end face using the TPP 3D printing method. The light propagating in the SMF is first reflected at the interface between the SMF and air and afterward at the interface

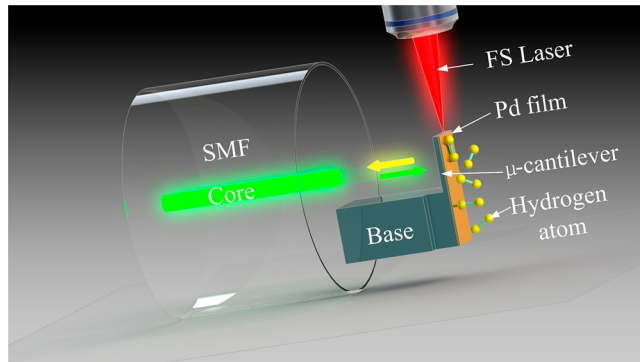


Figure 1. Schematic diagram of the hydrogen sensor based on a polymer μ -cantilever with Pd film on the fiber tip.

between the air and the lower surface of the μ -cantilever. These two reflections are combined to generate an interference signal. The expansion of the Pd lattices after hydrogen absorption stretches and deforms the suspended μ -cantilever, resulting in the change of the cavity length of the FPI. The dip wavelength observed in the reflection spectrum can be used to trace the μ -cantilever deformation. The low elastic modulus of the polymer can provide adequate deformation of the cantilever that ensures the high sensitivity of this sensor. By coating a \sim 120 nm thick Pd film onto a 3 μ m thick polymer μ -cantilever, we could achieve a high sensitivity (ca. -2 nm %⁻¹) and a short response time (13.5 s). The proposed device therefore rapidly detects low hydrogen concentrations at a minimal volume. Indeed, the aforementioned characteristics make it promising for medical and biological applications.

2. RESULTS AND DISCUSSION

2.1. Theoretical Basis. As a material extremely sensitive to hydrogen, Pd has the ability to absorb 900 \times its volume of hydrogen. Upon hydrogen exposure, the Pd film adsorbs and dissociates the hydrogen atoms at its surface, and the newly formed atoms rapidly diffuse into the interior of the Pd film to form PdH_x until reaching equilibrium. The fact that the formation of PdH_x will lead to the increase of the Pd lattice constant value has been proven using the calculation method based on density functional theory (DFT); for instance, Wang et al. and Wu et al. have obtained lattice growth rates of 4.2 and 1.98–5.99%, respectively.^{47,48} We coated the upper surface of the polymer μ -cantilever with a Pd film to form a bimaterial cantilever. The polymer was chosen to be the structural layer as it exhibits excellent mechanical properties compared to the intrinsic material of silica fiber. Since the polymer material is not sensitive to hydrogen, and the absorption of hydrogen induces a volumetric expansion of the Pd layer, resulting a differential strain between the Pd and polymer layers; thus, the cantilever is bent downward toward the fiber end facet. The polymer μ -cantilever and the fiber end facet act as two partially reflective mirrors and form a FP cavity. This deflection of the μ -cantilever is equivalent to the reduction in the cavity length. The relationship between the cavity length reduction (ΔL) and the dip wavelength shift ($\Delta\lambda$) follows $\Delta\lambda/\lambda = \Delta L/L$, where λ is the wavelength of the traced dip and L is the cavity length. Therefore, the H₂ concentration encoded in the μ -cantilever deflection can be extracted by directly measuring the dip wavelength shift of the FP cavity. The process is reversed when the external hydrogen concentration is reduced and hydrogen atoms recombine at the surface to become molecules again.⁴⁹

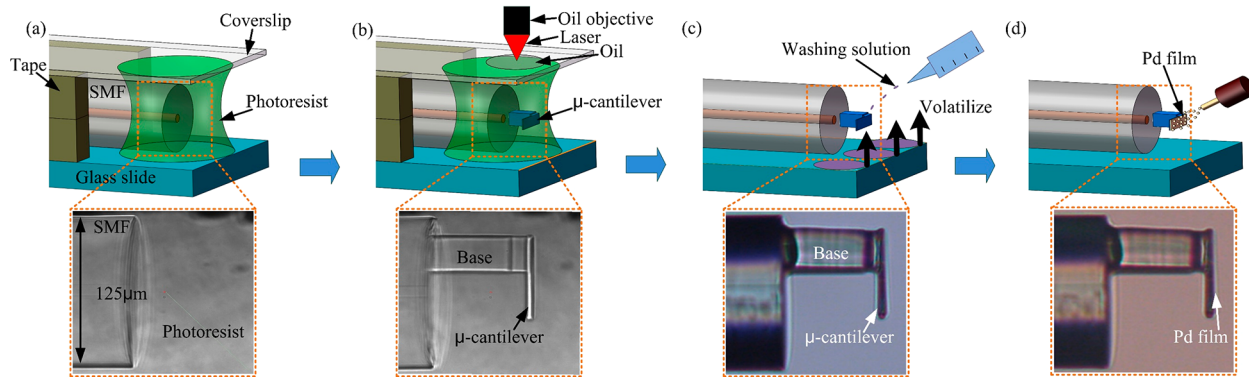


Figure 2. Flowchart of the device fabrication. (a) The flat end of the optical fiber is immersed in the negative photoresist, and the coverslip is used to isolate the photoresist from the oil and protect the objective lens. (b) FS-laser μ -cantilever polymerization. Scanning from the side of the optical fiber greatly reduces the preparation time of the samples. (c) A mixed solution (acetone/isopropanol 1:4) is used to wash the residual photoresist without polymerization. (d) The Pd film is coated on the μ -cantilever by magnetron sputtering.

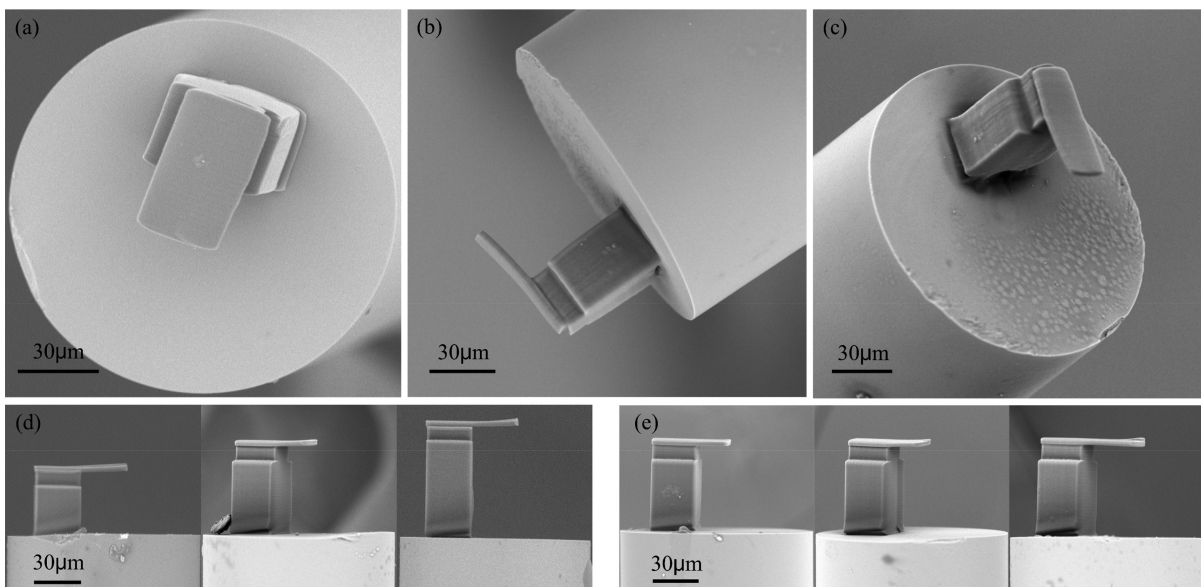


Figure 3. Scanning electron microscopy image of the polymer μ -cantilever on the fiber tip fabricated using the TPP technique. (a–c) The polymer μ -cantilever viewed from different angles, showing the details of the μ -cantilever on the 125 μ m diameter optical fiber. The edge of the base is 10 μ m away from the core to improve the reflectivity without affecting the sensitivity. (d) Polymer μ -cantilevers with different base heights (40, 60, and 80 μ m). (e) Polymer μ -cantilevers with different lengths (20, 30, and 40 μ m).

Assuming that the Young's moduli of the polymer and the Pd film do not change appreciably during the adsorption, the cantilever bending can be expressed as

$$Z = 3(\alpha_{\text{Pd}} - \alpha_{\text{Can}}) \left(\frac{t_{\text{Pd}} + t_{\text{Can}}}{t_{\text{Can}}^2 K} \right) CL^2 \quad (1)$$

where L is the length of the cantilever and $t_{i=\text{Pd,Can}}$ and $\alpha_{i=\text{Pd,Can}}$ are the layer thicknesses and expansion coefficients, respectively, with the subscripts referring to the Pd film and μ -cantilever. C is the equilibrium concentration of the hydrogen atoms inside the Pd, and K is Sievert's coefficient. Based on eq 1, a larger cantilever deflection can be obtained for a thinner cantilever at the same hydrogen concentration. If the hydrogen sensitivity of the sensor is defined as the ratio of the dip wavelength shift to hydrogen concentration, a thinner cantilever provides a higher sensitivity. Limited by the low stiffness of the polymer material, the thickness of the μ -cantilever was optimized to be $\sim 3 \mu\text{m}$ to ensure that the

spectral contrast and sensitivity are both as large as possible. The utilization of thicker Pd films is another alternative method to improve the hydrogen sensitivity but at the expense of a slower response speed.⁵⁰ In our case, the thickness of the Pd film is optimized at $\sim 120 \text{ nm}$ to maximize the response speed while still ensuring a high sensitivity.

2.2. Fabrication. The fabrication flowchart is illustrated in Figure 2. For step 1, a conventional SMF with a diameter of 125 μm is first cleaved and placed on the glass slide. Then, the fiber tip is immersed in a negative photoresist (purchased from Zhichu Optics Co., Ltd., Shenzhen, China), which is composed of a photoinitiator (IGR-369, Ciba-Geigy) with a mole ratio of 2.5%; monomer (SR444, SR368, and SR454 from Sartomer) with molar ratios of 40, 30, and 25%, respectively; 4-hydroxyanisole (MEHQ, from Sigma-Aldrich) with a mole ratio of 0.5%; and tetraethyl thiuram disulfide (TED from Sigma-Aldrich) with a mole ratio of 2.0%. Two layers of tape are used as spacers on each side of the fiber to prevent the coverslip from pressing against the fiber. The optical

microscopy image of the fiber tip immersed in a negative photoresist is shown in the lower part of Figure 2a. For step 2, as shown in Figure 2b, the sample was mounted on a 3D air-bearing stage (Aerotech) for the polymerization of the structure. The polymerization process employs a fs laser with a pulse width of 250 fs, a central wavelength of 1026 nm, and a pulse repetition rate of 200 kHz. An oil-immersion objective lens of 63 \times magnification (NA = 1.4) was selected to increase the smoothness of the structure. The power of the fs laser was 2 mw, and a scanning velocity of 300 $\mu\text{m s}^{-1}$ was selected to reduce the fabrication time. As shown in the lower part of Figure 2b, the μ -cantilever was polymerized on the fiber tip. For step 3, after polymerization the sample was immersed in an acetone and isopropyl alcohol mixture (1:4) for about 1 min to wash away any residual photoresist. After washing, the μ -cantilever was successfully printed on the fiber tip, as shown in Figure 2c. For step 4, the upper surface of the μ -cantilever was plated with Pd using a magnetron sputtering apparatus over 20 min (55 mA, 433 V, and 23 W). In order to improve the uniformity of the Pd film, it was necessary to keep the μ -cantilever perpendicular to the sputtering direction of the Pd target. Since it cannot be avoided that the end face of the optical fiber is coated by Pd during the sputtering process, we chose a Pd film with a thickness of 120 nm. This not only provides a high sensitivity but also makes removal of the Pd film easier by ablation with the fs laser. The lower part of Figure 2d shows the side view of the μ -cantilever coated with the Pd film.

2.3. Characterization. Figures 3a–e show a series of scanning electron microscope (SEM) images of the polymer μ -cantilever. The polymerized μ -cantilever can be clearly distinguished. It basically consists of two parts. At the bottom, the base structure is a $30 \times 30 \mu\text{m}$ square of the cross-sectional area with a variable height. The $30 \times 30 \mu\text{m}$ cross section was used to increase the adhesion between the fiber end face and the lever support. At the top, the μ -cantilever is attached to the base with estimated dimensions of a $20 \mu\text{m}$ width and a $3 \mu\text{m}$ thickness with a variable length. The SEM images in Figure 3a–c show a relatively smooth cantilever surface and good parallelism between the fiber end face and the lever. All these characteristics are helpful to increase both the intensity of the reflected light and the sensitivity of the device to deformation. In order to optimize the sensor performance, cantilevers of different sizes were fabricated and characterized. SEM images of three samples with base heights of 40, 60, and 80 μm are shown in Figure 3d. The parallelism between the polymer μ -cantilever and the end face of the optical fiber remains basically the same as the height increases, which shows the flexibility and reliability of the TPP fabrication. The tests revealed an optimum base height of 60 μm . Figure 3e shows the SEM images of three samples with different cantilever lengths of 20, 30, and 40 μm . Theoretically, even though small thickness and large length values enhance the sensitivity, the parallelism between the μ -cantilever and the fiber end face will be significantly impaired by the length increasing.

The reflection spectrum was measured using a broadband light source (BBS) with an optical spectrum analyzer (OSA), as shown in Figure 4a. The interference pattern can be explained by a three-beam interference induced by the fiber end face, the lower surface, and the upper surface of the μ -cantilever. The space between the fiber end face and the lower surface of the μ -cantilever forms an air microcavity (FPI1) with a length L_{Air} . The lower surface and the upper surface of the μ -

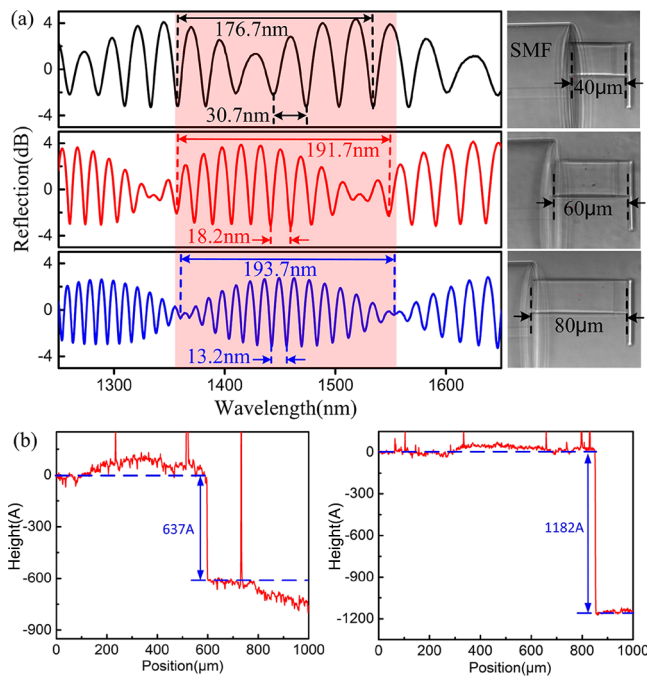


Figure 4. (a) Optical microscopy images of cantilevers with different heights and their corresponding reflection spectrum. The larger envelope is the FSR of FPI2, and the smaller FSR corresponds to FPI1. (b) The thickness of the Pd film was measured by a step profiler. The left figure and the right plots are the Pd film thickness after coating for 10 and 20 min, respectively.

cantilever form a polymer microcavity (FPI2) with a length L_{Poly} . Finally, the fiber end face and the upper surface of the μ -cantilever form a mixed microcavity (FPI3) with a length $L_{\text{Air}} + L_{\text{Poly}}$. In our case, the optical intensity of FPI3 is relatively low compared to those of FPI1 and FPI2. The free spectral range (FSR) of FPI1 and FPI2 can be calculated by eq 2

$$\text{FSR} = \frac{\lambda^2}{2nL} \quad (2)$$

where λ is the dip wavelength, L is the cavity length, and n is the refractive index of the medium in the cavity.

To optimize the structural parameters, we performed spectral tests on diverse μ -cantilevers with different base heights. The corresponding results of the reflection spectra are shown in Figure 4a. The refractive index of the employed polymer is ~ 1.53 .³³ Based on the FSR of FPI2 from the reflection spectra of the μ -cantilever with different base heights in Figure 4a, the thickness of the polymer cantilever calculated with eq 2 is $\sim 3 \mu\text{m}$. This thickness is consistent with the designed thickness, indicating the high accuracy of TPP. It is clear that increasing the base height leads to the reduced interference fringe visibility of the FPI, while a shorter base height increases the shift range and the spectrum contrast. However, if the length of the air cavity is too small, the polymer structure will easily fall off when the washing solution volatilizes due to the solution surface tension between the μ -cantilever and the fiber end face. Therefore, to simplify the device fabrication process without affecting the spectral contrast and sensitivity, we chose a 60 μm height and a $30 \times 30 \mu\text{m}$ sized μ -cantilever.

During the Pd coating process by magnetron sputtering, the Pd film was simultaneously deposited on the glass slide and the μ -cantilever. As shown in Figure 4b, we measured the thickness

of the Pd film on the glass slide after a 10 and 20 min coating process (55 mA, 433 V, and 23 W). The measurements performed with a step profiler recorded 63.7 and 118.2 nm heights, respectively. The thickness of the Pd film after the 20 min coating was almost double that of the 10 min coating, which proves that the magnetron sputtering process is precise and time-dependent. Furthermore, we estimated the relationship between the coating time and the Pd film thickness, obtaining a deposition rate of $\sim 6 \text{ nm min}^{-1}$.

2.4. Hydrogen Measurement. The setup used for testing and analyzing the device's sensitivity to hydrogen is depicted in Figure 5, where a simulated biological environment is

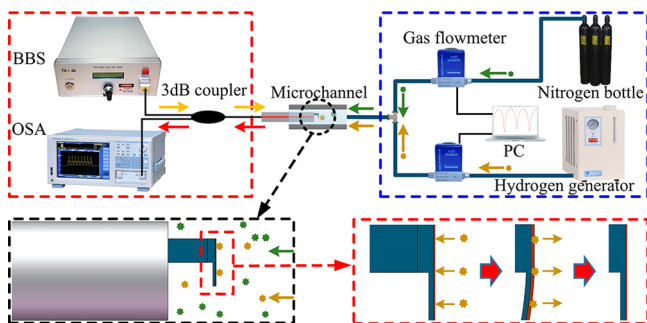


Figure 5. Experimental setup for hydrogen measurement in a microchannel. The content of nitrogen and hydrogen in the microchannel is controlled by two flowmeters. The lower part of the figure shows how the expansion of the Pd film causes the polymer cantilever to bend and return to its original position.

proposed. The probe sensor was inserted into a $500 \mu\text{m}$ diameter channel. The hydrogen produced by a hydrogen generator was mixed with nitrogen through three microchannel plastic pipes. The third microchannel served as the output channel for the mixture gas, and the sensor was fitted inside it. The hydrogen concentration in the mixed gas was controlled by two flowmeters (Seven Star, D07). The reflection spectrum was monitored in real time using a BBS and an OSA. The sensor was exposed to hydrogen concentrations ranging from 0 to 4.5% (v/v) with steps of 0.5% (v/v) at a temperature of 23.5 °C. Figure 6a gives the reflection spectrum of the Pd-coated μ -

cantilever while increasing the hydrogen concentration. It was found that the reflection spectrum is shifted toward the shorter wavelength when hydrogen started to flow into the microchannel, and the total shift of the dip wavelength near 1546 nm was ca. -8 nm when the hydrogen concentration rose from 0 to 4.5%. The dip wavelength vs the hydrogen concentration was then plotted, as shown in Figure 6b. An exponential function is fitted through the points. The wavelength shift is a nonlinear function of the hydrogen concentration, confirming Sievert's law.⁵¹ It is important to note that the sensitivity increases when the hydrogen concentration decreases.

In order to test the repeatability of this hydrogen sensor, three cycles of hydrogen concentration tests were conducted, and the corresponding dip wavelength blue shift is plotted in Figure 7. The total dip wavelength blue shifts of the three

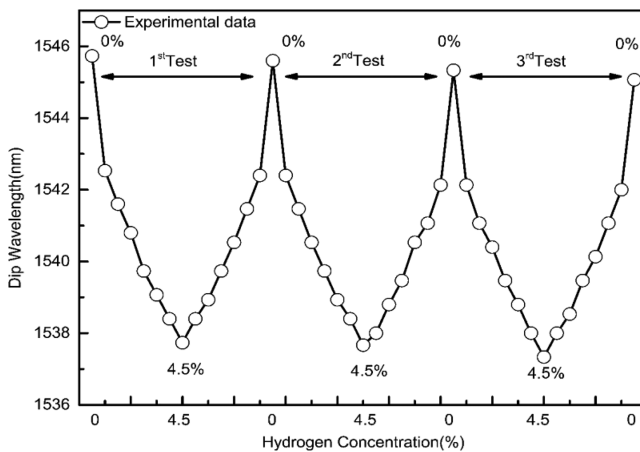


Figure 7. Three cycles of hydrogen concentration tests. The total dip wavelength blue shifts for the three measurements are 8.0, 7.9, and 8.0 nm.

measurements are 8.0, 7.9, and 8.0 nm, respectively. The dip wavelength is relatively stable at each hydrogen concentration whether the hydrogen concentration increases or decreases. The results show that the measurements with this hydrogen sensor are highly reproducible. As for the slight difference of dip wavelength blue shift in the three tests, we believe that it

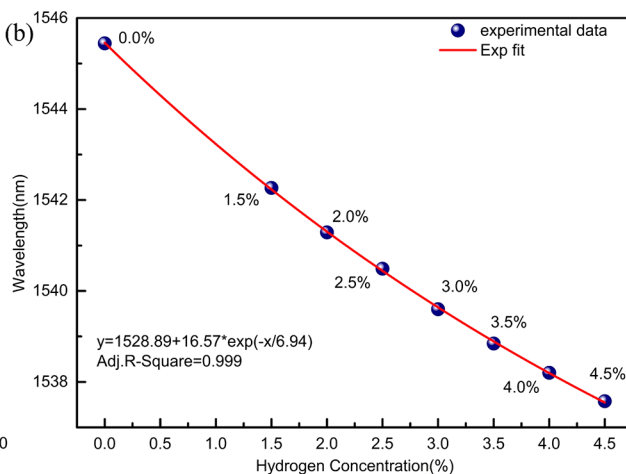
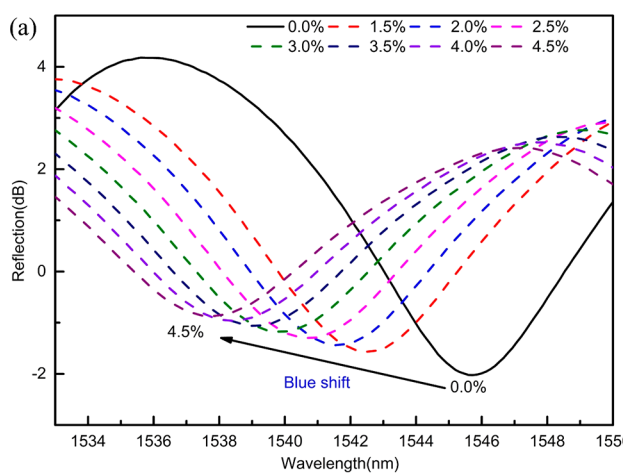


Figure 6. Response of the Pd-coated sensor to hydrogen with different hydrogen concentrations (v/v). (a) Reflection spectrum of the μ -cantilever at different hydrogen concentrations. (b) Dip wavelength vs the hydrogen concentration (v/v). The line through the points is a fit with an exponential function.

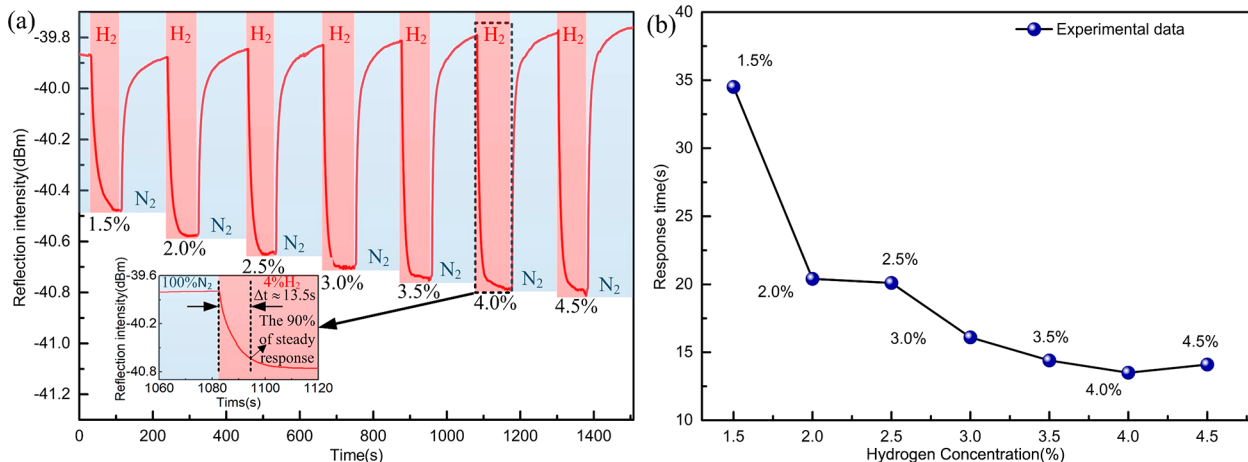


Figure 8. Response time of the sensor vs hydrogen concentration (v/v). (a) The intensity of the reflected light at the 1515 nm wavelength varies with time under the alternation of hydrogen and nitrogen. (b) The response time of the sensor at each measured hydrogen concentration.

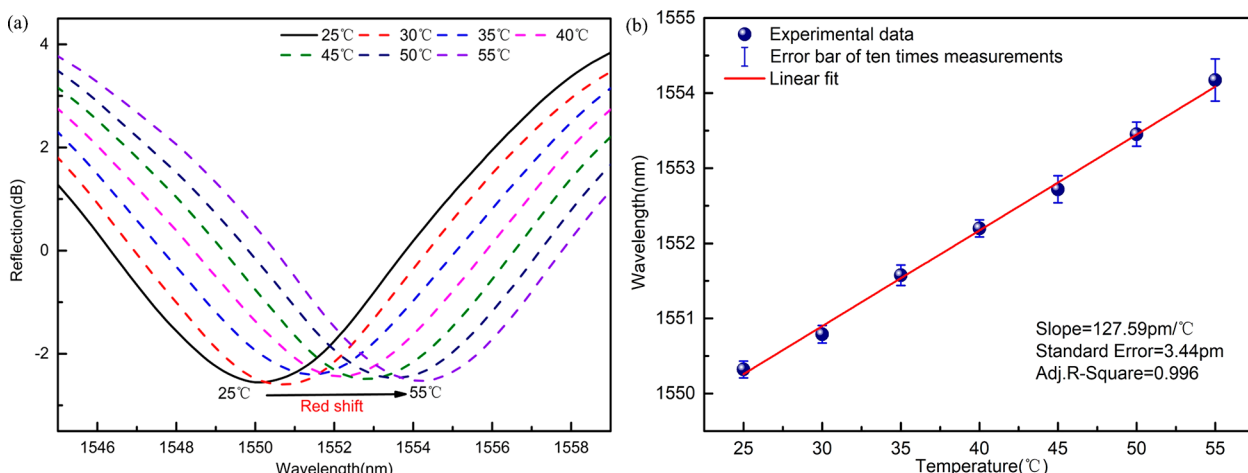


Figure 9. Temperature response of the polymer μ -cantilever, which indicates a linear relationship between the dip wavelength and the temperature. (a) Reflection spectra red shift as the temperature increases from 25 to 55 °C. (b) Data and a linear fit of the dip wavelength vs temperature. The standard deviation was calculated from ten measurements at each temperature.

could be caused by a difference in the hydrogen distribution uniformity in the microchannel.

To investigate the temporal response of the hydrogen sensor, an OSA was set up to scan at the single wavelength of 1515 nm, which is located at the fwhm (full at width half-maximum) of the reflection spectrum and has the largest slope. It is used to record the change in the reflected light intensity caused by the change in the hydrogen concentration. The device was cycled between different hydrogen concentrations and pure nitrogen, as shown in Figure 8a. It can be seen that the device response is repeatable for hydrogen concentrations ranging from 0 to 4.5% (v/v), and the reflected light intensity is restored every time to its initial value. It has to be noted that the response time is shorter than the recovery time. The reasons for this behavior are that the processes of absorption and dissociation of the hydrogen molecules and their diffusion into the Pd film are fast. However, once the hydrogen binds the Pd film it is firmly coupled with it, causing a slow diffusion out of the Pd film. The response time is defined as the time interval for the sensor to reach 90% of its steady response; according to this, the sensor response time is estimated to be ~ 13.5 s at 4% (v/v) hydrogen concentration. It is much faster than those of FBGs,^{24,25} SPR,^{16–18} and other hydrogen

sensors,^{19,20,22,23} which is very beneficial to the requirement of measuring speed for medical and biological applications. The response time vs the hydrogen concentration is plotted in Figure 8b. According to the Langmuir theory of the adsorption isotherm suitable for gas adsorption on a solid surface, the fraction of the Pd surface sites occupied by the hydrogen atom is proportional to the square root of the partial pressure of hydrogen in the environment.⁵² When the hydrogen concentration is low, the rate of hydrogen atom diffusion to the interior of the Pd film is slow due to the low fraction of the Pd surface sites occupied by the hydrogen atoms, resulting in the long response time, i.e., ~ 34.5 s at 1.5% (v/v) hydrogen concentration. With the increase in the external hydrogen concentration, the diffusion rate increases as the fraction of the Pd surface sites occupied by the hydrogen atoms, giving rise to the reduced response time. When the hydrogen concentration reaches 3%, the surface of the Pd film is saturated with hydrogen, and the diffusion rate of the hydrogen atom to the interior of the Pd film tends and the response time tend to be stable. Above 3%, in the case that the diffusion rate is basically stabilized, the response time increases slightly as more hydrogen atoms need to be diffused into the interior Pd film. Maintaining a short response time at a high hydrogen

concentration is of great significance for the fast concentration control in hydrogen medical treatment.

2.5. Temperature Measurement. To study the performance of the sensor for a general biomedical environment, the effect of temperature was investigated by placing the device into an oven in air and gradually increasing the temperature from 25 to 55 °C by 5 °C steps. The temperature was constantly maintained for 15 min at each step. The dip wavelength (~ 1550 nm) was used to monitor the effect of the temperature during the experiment. The evolution of the reflection spectrum with respect to temperature is shown in Figure 9a. The dip wavelength was observed to red shift with increasing temperatures. The dip wavelength shift of the FPI spectrum with temperature can be expressed by the following equation

$$\frac{d\lambda}{dT} = \frac{2}{k} \left(\frac{dn}{dT} L + \frac{dL}{dT} n \right) \quad (3)$$

where λ is the dip wavelength, k is an integer representing the order of the interference spectrum, $\frac{dn}{dT}$ is the thermo-optic coefficient of the medium in the cavity, and $\frac{dL}{dT}$ is the thermo-expansion coefficient of the polymer. The interference spectrum of FPII was used to track the deflection changes of the polymer μ -cantilever. Both the thermo-optical effect and the thermal expansion effect contributed to the shift of the interference spectrum when the ambient temperature was increased. However, because the FPII is filled with air, the refractive index of air barely changes with the increase in temperature. Therefore, we believe the dominant reason is that the thermal expansion of the polymer base of the μ -cantilever led to the increase of the cavity length.

Figure 9b illustrates the linear fit of the dip wavelength vs temperature and the standard deviation from ten measurements at each temperature, achieving a sensitivity of ~ 128 pm $^{\circ}\text{C}^{-1}$ with a standard error of 3.44 pm. When the temperature is below 50 °C, the response of the sensor is relatively stable, with the error bar of 0.1 nm calculated from ten measurements. As the temperature increases above 50 °C, the error bar presents a slight increase, which may be caused by the temperature instability of electric ovens at high temperatures. It should be noted that this polymer μ -cantilever has achieved a relatively low temperature cross sensitivity (ca. -0.064% $^{\circ}\text{C}^{-1}$) compared with other fiber hydrogen sensors based on long-period gratings (ca. -0.7% $^{\circ}\text{C}^{-1}$ ⁵³ and FBG ($\sim 4\%$ $^{\circ}\text{C}^{-1}$)⁵⁴). In addition to temperature crosstalk, Pd-based sensors are subject to crosstalk from other active gases in the mixture due to their good catalytic performance. However, this issue can be mitigated by replacing pure Pd with Pd alloys⁵⁵ or coating the protective layer.⁵⁶

3. CONCLUSIONS

We demonstrate a new hydrogen sensor based on a polymer μ -cantilever coated with a Pd film on a fiber tip. The μ -cantilever was fabricated by TPP 3D lithography on the fiber tip, which provided high sensitivity for hydrogen sensing due to its low stiffness while maintaining low temperature cross sensitivity. It presented a high hydrogen sensitivity, and the total shift of the dip wavelength near 1546 nm was ca. -8 nm when the hydrogen concentration rose from 0% to 4.5%. Its properties are of great significance for the precise control of hydrogen concentration in therapy. Moreover, the response time of the

sensor is very short, which can meet the requirements of immediacy in medical and biological applications. Compared with the existing commercial hydrogen sensors, such as those that convert the hydrogen concentration change into electrical signals, our sensor provides an ultracompact optical solution for fast and highly sensitive hydrogen concentration measurements in explosive or space-limited environments. We believe that such a hydrogen sensor with a polymer μ -cantilever will find applications in medical and biological hydrogen detection and environmental safety, owing to its microsize, high sensitivity, and fast response. In addition to providing an ultracompact optical solution for fast and highly sensitive hydrogen measurement, the polymer μ -cantilever fiber sensor can be used for diverse medical and biological sensing applications by replacing Pd with other functional materials.

ASSOCIATED CONTENT

Supporting Information

The Supporting Information is available free of charge at <https://pubs.acs.org/doi/10.1021/acsami.0c06179>.

Fabrication process of the polymer μ -cantilever with Pd film coated on the fiber tip; 3D modeling of the polymer μ -cantilever; slicing and scanning path settings; schematics of the geometrical arrangement of the fiber tip, photoresist, glass slide, refractive index matching oil, and objective lens in two-photon polymerization; removal of the residual photoresist; and coating method for the Pd film on the upper surface of the μ -cantilever (PDF)

AUTHOR INFORMATION

Corresponding Authors

Changrui Liao – Guangdong and Hong Kong Joint Research Centre for Optical Fiber Sensors and Key Laboratory of Optoelectronic Devices and Systems of the Ministry of Education and Guangdong Province, College of Physics and Optoelectronic Engineering, Shenzhen University, Shenzhen 518060, China;
 orcid.org/0000-0003-3669-5054; Email: ciao@szu.edu.cn

Giovanni Dietler – Laboratory of Physics of Living Matter, IPHYS, Ecole Polytechnique Fédérale de Lausanne (EPFL), CH-1015 Lausanne, Switzerland; Email: giovanni.dietler@epfl.ch

Authors

Cong Xiong – Guangdong and Hong Kong Joint Research Centre for Optical Fiber Sensors and Key Laboratory of Optoelectronic Devices and Systems of the Ministry of Education and Guangdong Province, College of Physics and Optoelectronic Engineering, Shenzhen University, Shenzhen 518060, China;
 orcid.org/0000-0003-4621-9270

Jiangtao Zhou – Laboratory of Physics of Living Matter, IPHYS, Ecole Polytechnique Fédérale de Lausanne (EPFL), CH-1015 Lausanne, Switzerland

Meng Zhu – Guangdong and Hong Kong Joint Research Centre for Optical Fiber Sensors and Key Laboratory of Optoelectronic Devices and Systems of the Ministry of Education and Guangdong Province, College of Physics and Optoelectronic Engineering, Shenzhen University, Shenzhen 518060, China

Ying Wang – Guangdong and Hong Kong Joint Research Centre for Optical Fiber Sensors and Key Laboratory of Optoelectronic Devices and Systems of the Ministry of Education and Guangdong Province, College of Physics and Optoelectronic

Engineering, Shenzhen University, Shenzhen 518060, China;
✉ orcid.org/0000-0001-8020-3622

Shen Liu — Guangdong and Hong Kong Joint Research Centre for Optical Fiber Sensors and Key Laboratory of Optoelectronic Devices and Systems of the Ministry of Education and Guangdong Province, College of Physics and Optoelectronic Engineering, Shenzhen University, Shenzhen 518060, China
Chi Li — Guangdong and Hong Kong Joint Research Centre for Optical Fiber Sensors and Key Laboratory of Optoelectronic Devices and Systems of the Ministry of Education and Guangdong Province, College of Physics and Optoelectronic Engineering, Shenzhen University, Shenzhen 518060, China

Yunfang Zhang — Guangdong and Hong Kong Joint Research Centre for Optical Fiber Sensors and Key Laboratory of Optoelectronic Devices and Systems of the Ministry of Education and Guangdong Province, College of Physics and Optoelectronic Engineering, Shenzhen University, Shenzhen 518060, China

Yuanyuan Zhao — Guangdong and Hong Kong Joint Research Centre for Optical Fiber Sensors and Key Laboratory of Optoelectronic Devices and Systems of the Ministry of Education and Guangdong Province, College of Physics and Optoelectronic Engineering, Shenzhen University, Shenzhen 518060, China

Zongsong Gan — Wuhan National Laboratory for Optoelectronics (WNLO), Huazhong University of Science and Technology (HUST), Wuhan 430074, China

Leonardo Venturelli — Laboratory of Physics of Living Matter, IPHYS, Ecole Polytechnique Fédérale de Lausanne (EPFL), CH-1015 Lausanne, Switzerland; ✉ orcid.org/0000-0002-9708-8170

Sandor Kasas — Laboratory of Physics of Living Matter, IPHYS, Ecole Polytechnique Fédérale de Lausanne (EPFL), CH-1015 Lausanne, Switzerland

Xuming Zhang — Department of Applied Physics, The Hong Kong Polytechnic University, Hong Kong, China; ✉ orcid.org/0000-0002-9326-5547

Yiping Wang — Guangdong and Hong Kong Joint Research Centre for Optical Fiber Sensors and Key Laboratory of Optoelectronic Devices and Systems of the Ministry of Education and Guangdong Province, College of Physics and Optoelectronic Engineering, Shenzhen University, Shenzhen 518060, China

Complete contact information is available at:
<https://pubs.acs.org/10.1021/acsami.0c06179>

Author Contributions

C.X., C. Liao, and J.Z. jointly conceived the idea. C.X. and C. Liao designed and fabricated the devices, built the experimental setup, and carried out the experiments. C.X., M.Z., C. Li, Y. Zhang, and Y. Zhao analyzed the data. Ying Wang, S.L., S.K., and Yiping Wang assisted with the theory. Z.G. synthesized the photoresist. C.X., C. Liao, J.Z., L.V., X.Z., and G.D. wrote the manuscript with contributions from all co-authors. All authors have given approval to the final version of the manuscript.

Notes

The authors declare no competing financial interest.

ACKNOWLEDGMENTS

The authors gratefully acknowledge Han Wu, Yanping Chen, and Bin Du for useful discussions. This study was supported by the National Natural Science Foundation of China (NSFC) (no. 61635007), the Natural Science Foundation of Guangdong Province (no. 2018B030306003), and the Science

and Technology Innovation Commission of Shenzhen (nos. K Q J S C X 2 0 1 7 0 7 2 7 1 0 1 9 5 3 6 8 0 a n d JCYJ20180507184503128).

REFERENCES

- (1) Ohsawa, I.; Ishikawa, M.; Takahashi, K.; Watanabe, M.; Nishimaki, K.; Yamagata, K.; Katsura, K.; Katayama, Y.; Asoh, S.; Ohta, S. Hydrogen Acts as a Therapeutic Antioxidant by Selectively Reducing Cytotoxic Oxygen Radicals. *Nat. Med.* **2007**, *13*, 688–694.
- (2) Carbonero, F.; Benefiel, A. C.; Gaskins, H. R. Contributions of the Microbial Hydrogen Economy to Colonic Homeostasis. *Nat. Rev. Gastroenterol. Hepatol.* **2012**, *9*, 504–518.
- (3) Fu, Y.; Ito, M.; Fujita, Y.; Ito, M.; Ichihara, M.; Masuda, A.; Suzuki, Y.; Maesawa, S.; Kajita, Y.; Hirayama, M.; Ohsawa, I.; Ohta, S.; Ohno, K. Molecular Hydrogen is Protective against 6-Hydroxydopamine-Induced Nigrostriatal Degeneration in a Rat Model of Parkinson's disease. *Neurosci. Lett.* **2009**, *453*, 81–85.
- (4) Katsuki, A.; Fukui, K. H₂ Selective Gas Sensor Based on SnO₂. *Sens. Actuators, B* **1998**, *52*, 30–37.
- (5) Bouchet, R.; Rosini, S.; Vitter, G.; Siebert, E. Solid-State Hydrogen Sensor Based on Acid-Doped Polybenzimidazole. *Sens. Actuators, B* **2001**, *76*, 610–616.
- (6) Baselt, D. R.; Frühberger, B.; Klaassen, E.; Cemalovic, S.; Britton, C. L., Jr.; Patel, S. V.; Mlsna, T. E.; McCorkle, D.; Warmack, B. Design and Performance of a Microcantilever-Based Hydrogen Sensor. *Sens. Actuators, B* **2003**, *88*, 120–131.
- (7) Liang, L.; Zuo, Y. F.; Wu, W.; Zhu, X. Q.; Yang, Y. Optofluidic Restricted Imaging, Spectroscopy and Counting of Nanoparticles by Evanescent Wave using Immiscible Liquids. *Lab Chip* **2016**, *16*, 3007–3014.
- (8) Antman, Y.; Clain, A.; London, Y.; Zadok, A. Optomechanical Sensing of Liquids Outside Standard Fibers using Forward Stimulated Brillouin Scattering. *Optica* **2016**, *3*, 510–516.
- (9) Tran, N. H. T.; Kim, J.; Phan, T. B.; Khym, S.; Ju, H. Label-Free Optical Biochemical Sensors via Liquid-Cladding-Induced Modulation of Waveguide Modes. *ACS Appl. Mater. Interfaces* **2017**, *9* (37), 31478–31487.
- (10) Xu, B.; Huang, J.; Xu, X.; Zhou, A.; Ding, L. Ultrasensitive NO Gas Sensor Based on the Graphene Oxide-Coated Long-Period Fiber Grating. *ACS Appl. Mater. Interfaces* **2019**, *11* (43), 40868–40874.
- (11) Xiao, A.; Huang, Y.; Zheng, J.; Chen, P.; Guan, B. O. An Optical Microfiber Biosensor for CEACAMS Detection in Serum: Sensitization by a Nanosphere Interface. *ACS Appl. Mater. Interfaces* **2020**, *12* (1), 1799–1805.
- (12) Tsvirkun, V.; Sivankutty, S.; Baudelle, K.; Habert, R.; Bouwmans, G.; Vanvincq, O.; Andresen, E. R.; Rigneault, H. Flexible Lensless Endoscope with a Conformationally Invariant Multi-Core Fiber. *Optica* **2019**, *6*, 1185–1189.
- (13) Ma, G.; Li, C.; Luo, Y.; Mu, R.; Wang, L. High Sensitive and Reliable Fiber Bragg Grating Hydrogen Sensor for Fault Detection of Power Transformer. *Sens. Actuators, B* **2012**, *169*, 195–198.
- (14) Schultz, A. M.; Brown, T. D.; Buric, M. P.; Lee, S.; Gerdes, K.; Ohodnicki, P. R. High Temperature Fiber-Optic Evanescent Wave Hydrogen Sensors using La-Doped SrTiO₃ for SOFC Applications. *Sens. Actuators, B* **2015**, *221*, 1307–1313.
- (15) Kabcum, S.; Channei, D.; Tuantranont, A.; Wisitsoraat, A.; Liewhiran, C.; Phanichphant, S. Ultra-Responsive Hydrogen Gas Sensors Based on PdO Nanoparticle-Decorated WO₃ Nanorods Synthesized by Precipitation and Impregnation Methods. *Sens. Actuators, B* **2016**, *226*, 76–89.
- (16) Bévenot, X.; Trouillet, A.; Veillas, C.; Gagnaire, H.; Clément, M. Surface Plasmon Resonance Hydrogen Sensor using an Optical Fibre. *Meas. Sci. Technol.* **2002**, *13*, 118.
- (17) Perrotton, C.; Javahiraly, N.; Slaman, M.; Dam, B.; Meyrueis, P. Fiber Optic Surface Plasmon Resonance Sensor Based on Wavelength Modulation for Hydrogen Sensing. *Opt. Express* **2011**, *19*, A1175–A1183.

- (18) Perrotton, C.; Westerwaal, R. J.; Javahiraly, N.; Slaman, M.; Schreuders, H.; Dam, B.; Meyrueis, P. A Reliable, Sensitive and Fast Optical Fiber Hydrogen Sensor Based on Surface Plasmon Resonance. *Opt. Express* **2013**, *21*, 382–390.
- (19) Sekimoto, S.; Nakagawa, H.; Okazaki, S.; Fukuda, K.; Asakura, S.; Shigemori, T.; Takahashi, S. A Fiber-Optic Evanescent-Wave Hydrogen Gas Sensor using Palladium-Supported Tungsten Oxide. *Sens. Actuators, B* **2000**, *66*, 142–145.
- (20) Villatoro, J.; Monzon-Hernandez, D. Fast Detection of Hydrogen with Nano Fiber Tapers Coated with Ultra Thin Palladium Layers. *Opt. Express* **2005**, *13*, 5087–5092.
- (21) Qi, Y.; Zhao, Y.; Bao, H.; Jin, W.; Ho, H. L. Nanofiber Enhanced Stimulated Raman Spectroscopy for Ultra-Fast, Ultra-Sensitive Hydrogen Detection with Ultra-Wide Dynamic Range. *Optica* **2019**, *6*, 570–576.
- (22) Wang, M.; Yang, M. H.; Cheng, J.; Dai, J. X.; Yang, M. W.; Wang, D. N. Femtosecond Laser Fabricated Micro Mach-Zehnder Interferometer with Pd Film as Sensing Materials for Hydrogen Sensing. *Opt. Lett.* **2012**, *37*, 1940–1942.
- (23) Xu, B.; Zhao, C. L.; Yang, F.; Gong, H. P.; Wang, D. N.; Dai, J. X.; Yang, M. G. Sagnac Interferometer Hydrogen Sensor Based on Panda Fiber with Pt-Loaded WO_3/SiO_2 Coating. *Opt. Lett.* **2016**, *41*, 1594–1597.
- (24) Dai, J.; Yang, M.; Chen, Y.; Cao, K.; Liao, H.; Zhang, P. Side-Polished Fiber Bragg Grating Hydrogen Sensor with $\text{WO}_3\text{-Pd}$ Composite Film as Sensing Materials. *Opt. Express* **2011**, *19*, 6141–6148.
- (25) Dai, J.; Yang, M.; Yang, Z.; Li, Z.; Wang, Y.; Wang, G.; Zhang, Y.; Zhuang, Z. Enhanced Sensitivity of Fiber Bragg Grating Hydrogen Sensor using Flexible Substrate. *Sens. Actuators, B* **2014**, *196*, 604–609.
- (26) Gu, F.; Zhang, L.; Zhu, Y.; Zeng, H. Free-Space Coupling of Nanoantennas and Whispering-Gallery Microcavities with Narrowed Linewidth and Enhanced Sensitivity. *Laser Photonics Rev.* **2015**, *9*, 682–688.
- (27) Liu, N.; Tang, M. L.; Hentschel, M.; Giessen, H.; Alivisatos, A. P. Nanoantenna-Enhanced Gas Sensing in a Single Tailored Nanofocus. *Nat. Mater.* **2011**, *10*, 631–636.
- (28) Wang, M.; Yang, M.; Cheng, J.; Zhang, G.; Liao, C. R.; Wang, D. N. Fabry-Pérot Interferometer Sensor Fabricated by Femtosecond Laser for Hydrogen Sensing. *IEEE Photonics Technol. Lett.* **2013**, *25*, 713–716.
- (29) Xie, Z. W.; Feng, S. F.; Wang, P. J.; Zhang, L. S.; Ren, X.; Cui, L.; Zhai, T. R.; Chen, J.; Wang, Y. L.; Wang, X. K.; Sun, W. F.; Ye, J. S.; Han, P.; Klar, P. J.; Zhang, Y. Demonstration of a 3D Radar-Like SERS Sensor Micro- and Nanofabricated on an Optical Fiber. *Adv. Opt. Mater.* **2015**, *3*, 1232–1239.
- (30) Gissibl, T.; Schmid, M.; Giessen, H. Spatial Beam Intensity Shaping using Phase Masks on Single-Mode Optical Fibers Fabricated by Femtosecond Direct Laser Writing. *Optica* **2016**, *3*, 448–451.
- (31) Nocentini, S.; Martella, D.; Parmeggiani, C.; Zanotto, S.; Wiersma, D. S. Structured Optical Materials Controlled by Light. *Adv. Opt. Mater.* **2018**, *6*, 1800167.
- (32) Wang, J.; Lin, C. P.; Liao, C. R.; Gan, Z. S.; Li, Z. Y.; Liu, S.; Xu, L.; Wang, Y.; He, J.; Wang, Y. P. Bragg Resonance in Microfiber Realized by Two-Photon Polymerization. *Opt. Express* **2018**, *26*, 3732–3737.
- (33) Li, C.; Liao, C. R.; Wang, J.; Li, Z. Y.; Wang, Y.; He, J.; Bai, Z. Y.; Wang, Y. P. Femtosecond Laser Microprinting of a Polymer Fiber Bragg Grating for High-Sensitivity Temperature Measurements. *Opt. Lett.* **2018**, *43*, 3409–3412.
- (34) Liao, C. R.; Li, C.; Wang, C.; Wang, Y.; He, J.; Liu, S.; Bai, Z. Y.; Gan, Z. S.; Wang, Y. P. High-Speed All-Optical Modulator Based on a Polymer Nanofiber Bragg Grating Printed by Femtosecond Laser. *ACS Appl. Mater. Interfaces* **2020**, *12* (1), 1465–1473.
- (35) Power, M.; Thompson, A. J.; Anastasova, S.; Yang, G. Z. A Monolithic Force Sensitive 3D Microgripper Fabricated on the Tip of an Optical Fiber Using 2-Photon Polymerization. *Small* **2018**, *14*, 1703964.
- (36) Alsharif, N.; Burkatsky, A.; Lissandrello, C.; Jones, K. M.; White, A. E.; Brown, K. A. Design and Realization of 3D Printed AFM Probes. *Small* **2018**, *14*, 1800162.
- (37) Wang, J.; He, Y.; Xia, H.; Niu, L. G.; Zhang, R.; Chen, Q. D.; Zhang, Y. L.; Li, Y. F.; Zeng, S. J.; Qin, J. H.; Lin, B. C.; Sun, H. B. Embellishment of Microfluidic Devices via Femtosecond Laser Micronanofabrication for Chip Functionalization. *Lab Chip* **2010**, *10*, 1993–1996.
- (38) Tian, Y.; Zhang, Y. L.; Ku, J. F.; He, Y.; Xu, B. B.; Chen, Q. D.; Xia, H.; Sun, H. B. High Performance Magnetically Controllable Microturbines. *Lab Chip* **2010**, *10*, 2902–2905.
- (39) Kelemen, L.; Lepera, E.; Horvath, B.; Ormos, P.; Osellame, R.; Martinez Vazquez, R. Direct Writing of Optical Microresonators in a Lab-on-a-Chip for Label-Free Biosensing. *Lab Chip* **2019**, *19*, 1985–1990.
- (40) Spagnolo, B.; Brunetti, V.; Lemenager, G.; De Luca, E.; Sileo, L.; Pellegrino, T.; Paolo Pompa, P.; De Vittorio, M.; Pisanello, F. Three-Dimensional Cage-Like Microscaffolds for Cell Invasion Studies. *Sci. Rep.* **2015**, *5*, 10531.
- (41) Hippler, M.; Lemma, E. D.; Bertels, S.; Blasco, E.; Barner-Kowollik, C.; Wegener, M.; Bastmeyer, M. 3D Scaffolds to Study Basic Cell Biology. *Adv. Mater.* **2019**, *31*, 1808110.
- (42) Hu, Y. L.; Wang, Z. Y.; Jin, D. D.; Zhang, C. C.; Sun, R.; Li, Z. Q.; Hu, K.; Ni, J. C.; Cai, Z.; Pan, D.; Wang, W. W.; Zhu, W. L.; Li, J. W.; Wu, D.; Zhang, L.; Chu, J. R. 4D Printing: Botanical-Inspired 4D Printing of Hydrogel at the Microscale. *Adv. Funct. Mater.* **2020**, *30*, 2070026.
- (43) Lao, Z. X.; Zheng, Y. Y.; Dai, Y. C.; Hu, Y. L.; Ni, J. C.; Ji, S. Y.; Cai, Z.; Smith, Z. J.; Li, J. W.; Zhang, L.; Wu, D.; Chu, J. R. Nanogap Plasmonic Structures Fabricated by Switchable Capillary-Force Driven Self-Assembly for Localized Sensing of Anticancer Medicines with Microfluidic SERS. *Adv. Funct. Mater.* **2020**, *30*, 1909467.
- (44) Xie, Z. W.; Gao, S. C.; Lei, T.; Feng, S. F.; Zhang, Y.; Li, F.; Zhang, J. B.; Li, Z. H.; Yuan, X. C. Integrated (De)Multiplexer for Orbital Angular Momentum Fiber Communication. *Photonics Res.* **2018**, *6*, 743–749.
- (45) Gissibl, T.; Thiele, S.; Herkommer, A.; Giessen, H. Two-Photon Direct Laser Writing of Ultracompact Multi-Lens Objectives. *Nat. Photonics* **2016**, *10*, 554–560.
- (46) Goeders, K. M.; Colton, J. S.; Bottomley, L. A. Microcantilevers: Sensing Chemical Interactions via Mechanical Motion. *Chem. Rev.* **2008**, *108*, 522–542.
- (47) Wang, Y.; Sun, S. N.; Chou, M. Y. Total-Energy Study of Hydrogen Ordering in PdH_x . *Phys. Rev. B: Condens. Matter Mater. Phys.* **1996**, *53*, 1–4.
- (48) Wu, X. J.; Li, Q. X.; Yang, J. L. Electronic Transport Properties of $\text{Pd}-\text{H}$ Junctions between Two PdH_x Electrodes: A Nonequilibrium Green's Function Study. *Phys. Rev. B: Condens. Matter Mater. Phys.* **2005**, *72*, 115438.
- (49) Lundstrom, I.; Armgarth, M.; Petersson, L. G. Physics with Catalytic Metal Gate Chemical Sensors. *Crit. Rev. Solid State Mater. Sci.* **1989**, *18*, 201–278.
- (50) Javahiraly, N. Review on Hydrogen Leak Detection: Comparison between Fiber Optic Sensors Based on Different Designs with Palladium. *Opt. Eng.* **2015**, *54*, 030901.
- (51) Hughes, R. C.; Bastasz, R. Low Energy Proton Detection by Pd Metal Insulator Semiconductor Diodes. *J. Appl. Phys.* **1988**, *64*, 6839–6844.
- (52) Sun, Y.; Wang, H. H. High-Performance, Flexible Hydrogen Sensors That Use Carbon Nanotubes Decorated with Palladium Nanoparticles. *Adv. Mater.* **2007**, *19*, 2818–2823.
- (53) Maier, R. R. J.; Jones, B. J. S.; Barton, J. S.; McCulloch, S.; Allsop, T.; Jones, J. D. C.; Bennion, I. Fibre Optics in Palladium-Based Hydrogen Sensing. *J. Opt. A: Pure Appl. Opt.* **2007**, *9*, S45–S59.
- (54) Trouillet, A.; Marin, E.; Veillas, C. Fibre Gratings for Hydrogen Sensing. *Meas. Sci. Technol.* **2006**, *17*, 1124–1128.
- (55) Petersson, L. G.; Dannetun, H. M.; Lundstrom, I. Hydrogen Detection during Catalytic Surface Evidence for Activated Lateral

Hydrogen Mobility in the Water-Forming Reaction on Pd. *Phys. Rev. Lett.* **1984**, *52*, 1806.

(56) Ngene, P.; Westerwaal, R. J.; Sachdeva, S.; Haije, W.; de Smet, L. C. P. M.; Dam, B. Polymer-Induced Surface Modifications of Pd-Based Thin Films leading to Improved Kinetics in Hydrogen Sensing and Energy Storage Applications. *Angew. Chem., Int. Ed.* **2014**, *53*, 12081–12085.